A CATALOG OF MIPSGAL DISK AND RING SOURCES

2010 The Astronomical Journal 139 1542

(http://iopscience.iop.org/1538-3881/139/4/1542)

The Astronomical Journal, 139:1542–1552, 2010 April doi:10.1088/0004-6256/139/4/1542

A CATALOG OF MIPSGAL DISK AND RING SOURCES

D. R. Mizuno[1], K. E. Kraemer[2], N. Flagey[3], N. Billot[4], S. Shenoy[5], R. Paladini[3], E. Ryan[6], A. Noriega-Crespo[3], and S. J. Carey[3]

[1] Institute for Scientific Research, Boston College, 140 Commonwealth Ave., Chestnut Hill, MA 02467-3862, USA; afrl.rvb.pa@hanscom.af.mil
[2] Air Force Research Laboratory, AFRL/RVBYB, 29 Randolph Road, Hanscom AFB, MA 10731, USA
[3] Spitzer Science Center, MS 220-6, California Institute of Technology, Pasadena, CA 91125, USA
[4] Infrared Processing and Analysis Center, MS 100-22, California Institute of Technology, Pasadena, CA 91125, USA
[5] Ames Research Center, MS 245-6, Moffett Field, CA 94035, USA
[6] Department of Astronomy, University of Minnesota, 116 Church St. S.E., Minneapolis, MN 55455, USA
Received 2009 October 9; accepted 2010 January 3; published 2010 March 11

ABSTRACT

We present a catalog of 416 extended, resolved, disk and ringlike objects as detected in the MIPSGAL 24 μm survey of the Galactic plane. This catalog is the result of a search in the MIPSGAL image data for generally circularly symmetric, extended "bubbles" without prior knowledge or expectation of their physical nature. Most of the objects have no extended counterpart at 8 μm or 70 μm, with less than 20% detections at each wavelength. For the 54 objects with central point sources, the sources are nearly always seen in all Infrared Array Camera bands. About 70 objects (16%) have been previously identified, with another 35 listed as *Infrared Astronomical Satellite* sources. Among the identified objects, those with central sources are mostly listed as emission-line stars, but with other source types including supernova remnants (SNRs), luminous blue variables, and planetary nebulae (PNe). The 57 identified objects (of 362) without central sources are nearly all PNe (∼90%), which suggests that a large fraction of the 300+ unidentified objects in this category are also PNe. These identifications suggest that this is primarily a catalog of evolved stars. Also included in the catalog are two filamentary objects that are almost certainly SNRs, and 10 unusual compact extended objects discovered in the search. Two of these show remarkable spiral structure at both 8 μm and 24 μm. These are likely background galaxies previously hidden by the intervening Galactic plane.

Key words: catalogs – infrared: ISM – planetary nebulae: general

Online-only material: machine-readable and VO table

1. INTRODUCTION

When a star evolves up the asymptotic giant branch (AGB), its atmosphere expands and cools. The ejected gas can condense into dust grains within the circumstellar shell, which may become quite bright in the infrared (IR), while at the same time often becoming sufficiently optically thick to hide the star itself in the optical. As the star continues to evolve and shed mass, it becomes a post-AGB object, and eventually a planetary nebula (PN) or supernova (SN). These objects at the end stages of the stellar life cycle are responsible for creating most of the dust in the universe (e.g., Gehrz 1989) and injecting it into the interstellar medium, where it can then form into new stars and planets. Because of the dust content of the circumstellar shells around AGB stars and in the ejecta of PNe and SNe, the IR is an ideal wavelength regime in which to identify new evolved objects. This is particularly true in the Galactic plane where high extinction in the optical limits searches to nearby sources. Previous IR surveys such as the Air Force Geophysics Laboratory (AFGL; Walker & Price 1975) and *Infrared Astronomical Satellite* (*IRAS*; Olnon et al. 1986) surveys found hundreds of AGB stars due to their dust emission, although they generally could not resolve the circumstellar structures around the stars.

Identification of new evolved star candidates and their circumstellar shells has recently been facilitated with the advent of high-resolution mid-infrared imaging surveys. While full characterization of the progenitors may require spectroscopy, IR imaging is often the easiest and most telescope-time efficient way to identify evolved stars, particularly along lines of sight with high extinction. Specifically, the *Spitzer* Legacy surveys of the inner Galaxy, MIPSGAL (Carey et al. 2009) with the Multiband Imaging Photometer for *Spitzer* (MIPS) instrument at 24 μm and 70 μm(Rieke et al. 2004), and the Galactic Legacy Infrared Mid-Plane Survey Extraordinaire (GLIMPSE; Benjamin et al. 2003), with the Infrared Array Camera (IRAC) at 3.6–8.0 μm (Fazio et al. 2004), provide high-resolution (1.″8–6″) imaging of the majority of the inner Galactic disk, which should include a large fraction of the evolved stars in the Milky Way. Ring and bubble structures associated with evolved stars, PNe, and supernova remnants (SNRs) are readily identifiable in these data sets. Indeed, several studies of rings found in the GLIMPSE archive, i.e., at 3.6–8.0 μm, have already been made, such as Phillips & Ramos-Larios (2008) or Churchwell et al. (2006), although these were primarily from massive young stars and only a few SNRs. Here, we present a catalog of ring and disk sources found in the MIPSGAL data at 24 μm.

2. IDENTIFICATION OF SOURCES

The MIPSGAL 24 μm mosaics (Mizuno et al. 2008; Carey et al. 2009) were searched by visual examination for candidate "bubble" objects. (Visual inspection is still the most reliable way to detect sets of extended objects; no automated procedure yet exists to replace the human eye.) The criteria for inclusion were as follows: (1) generally round shape with a hard-edged boundary, with either (2) an approximately flat "disk" profile, or (3) the presence of a ring or a partial ring, allowing some amount of regular or irregular structure or irregular shape. In particular, we excluded round and extended but centrally peaked objects: those of small angular size are either unresolved or barely resolved at the 6″ resolution of the MIPSGAL survey and

thus have uncertain underlying morphology; larger, and likely resolved, examples of such objects have also been excluded from the candidate set somewhat arbitrarily. In addition to the round extended objects specifically sought, we were also attentive to any compact extended objects that had a common morphology; we identified and included an ensemble of objects that have a bipolar or "two-lobed" appearance.

A total of 416 objects were selected. The objects were grouped, by a visual assessment of their morphology, into four primary categories. The first is objects with a detected central point source at 24 μm. The objects without central point sources are separately categorized as rings, disks, or two-lobed. Each group is further divided into subgroups depending on particular symmetry and regularity properties. Note that the groups and subgroups are defined entirely by the visual appearance of the objects; we make no a priori claim that these groupings represent underlying physical distinctions apart from the obvious morphology. In addition, two small additional categories are included: filamentary objects (two items, both identified as SNRs) and a miscellaneous category (10 objects) containing singular compact extended objects.

Objects with central point sources (group 1). The general morphology is almost invariably ringlike, which is not surprising as the visibility of a central source implies an optically thin shell. Figure 1 shows a few representative examples. The median angular size of these objects, about 44″, is approximately twice that of the objects lacking a visible 24 μm central source. Only three of objects lacking a central source are larger than 44″ (in a six times more numerous ensemble), so this difference indicates that these are a distinct population of objects apart from the visibility of the central source itself. *Regular* (1a) examples are, in gross features, axially symmetric or bilaterally symmetric. *Irregular* (1b) examples feature highly nonuniform or nonaxisymmetric ring brightness, or significant extended structure apart from the ring itself.

Rings (without central sources) (group 2). These are divided into three subcategories. *Rings* (2a) are complete rings with some allowed unevenness in ring brightness or morphology but no other significant structure. Included in this subcategory are both thin rings and the more common "thick ring" object type whose appearance is as a flat disk with a central depression. *Irregular rings* (2b) are objects featuring either a partial ring or a complete ring but with large variations in brightness or thickness around the ring. *Bilaterally symmetric rings* (2c) have an axis across which the ring has either symmetrically enhanced brightness or a change in shape such that the ring typically acquires a "D" shape on either side. Figure 2 shows examples of each of these three subcategories.

Disks (group 3). These have five subcategories: *flat* disks (3a) are axisymmetric, largely featureless disks with an essentially flat profile; "flat" is here assessed using a radial profile calculated for each disk from the 24 μm image data, consisting of an azimuthal average at each radius in (1.″25) pixel increments, and is defined as a less than 5% drop from the peak brightness at the third pixel radius in the profiles, i.e., a region about a resolution element wide in solid angle. Some minor structure is allowed as there are no truly featureless, flat disks. *Peaked* disks (3b) are axisymmetric but fail the flatness criterion in the radial profiles. Note that circularly symmetric but strongly peaked extended objects have generally been excluded from consideration for this catalog, so this subgroup is just a partial sampling of such objects. *Bilaterally symmetric* disks (3c) have a symmetry axis with enhanced brightness on either side; typically, these look like otherwise flat disks with a slot across the center. *Oblong* disks (3d) are featureless but have a slightly elliptical or elongated shape rather than round. *Irregular* disks (3e) have either pronounced asymmetric structure or irregular shape. Figure 3 shows examples of the disk subcategories. The flat and peaked examples also show horizontal profiles to demonstrate the distinction between these subgroups.

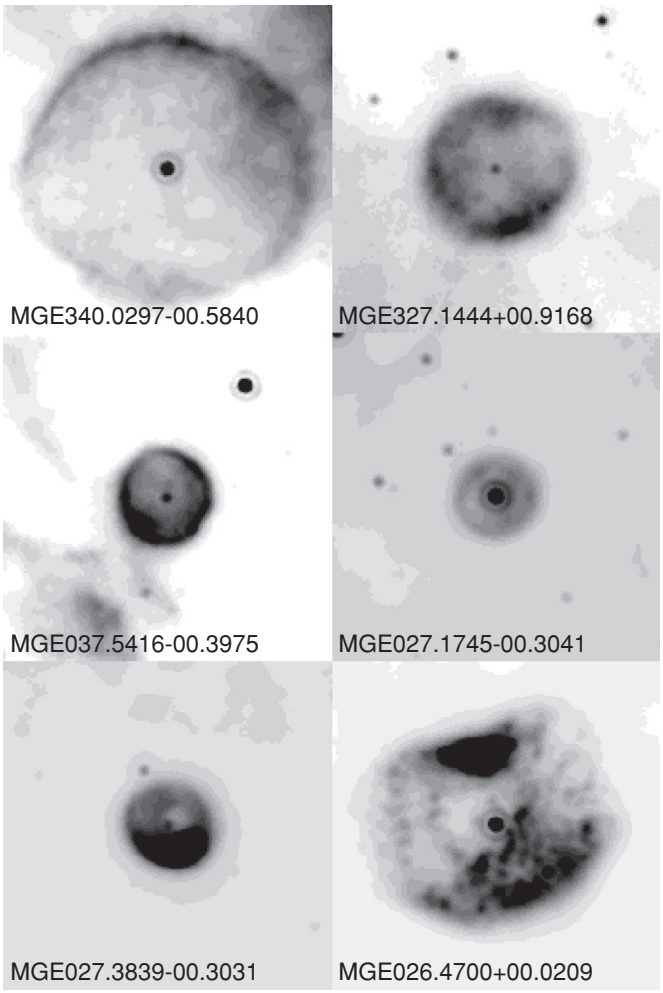

Figure 1. Examples of objects with central sources. The bottom row is "irregular" examples. Each panel is about 3.′3 across.

Two-lobed (group 4). Unlike the other categories, these objects are not primarily round. Rather, they consist of two small lobes typically separated by a much fainter lane perpendicular to the emission lobes. Figure 4 shows a few examples. One lobe is usually brighter than the other, presumably due to the viewing geometry. While many of the bilaterally symmetric rings and disks have a generally two-lobed appearance, this category contains objects that have a specific two-lobed boundary and no underlying disk.

Filamentary (group 5). This category includes localized, bounded objects with a primarily filamentary appearance, and contains just two objects which are identified as SNRs (Figure 5).

Miscellaneous (group 6). This category contains a small number of singular compact extended objects that were discovered in the

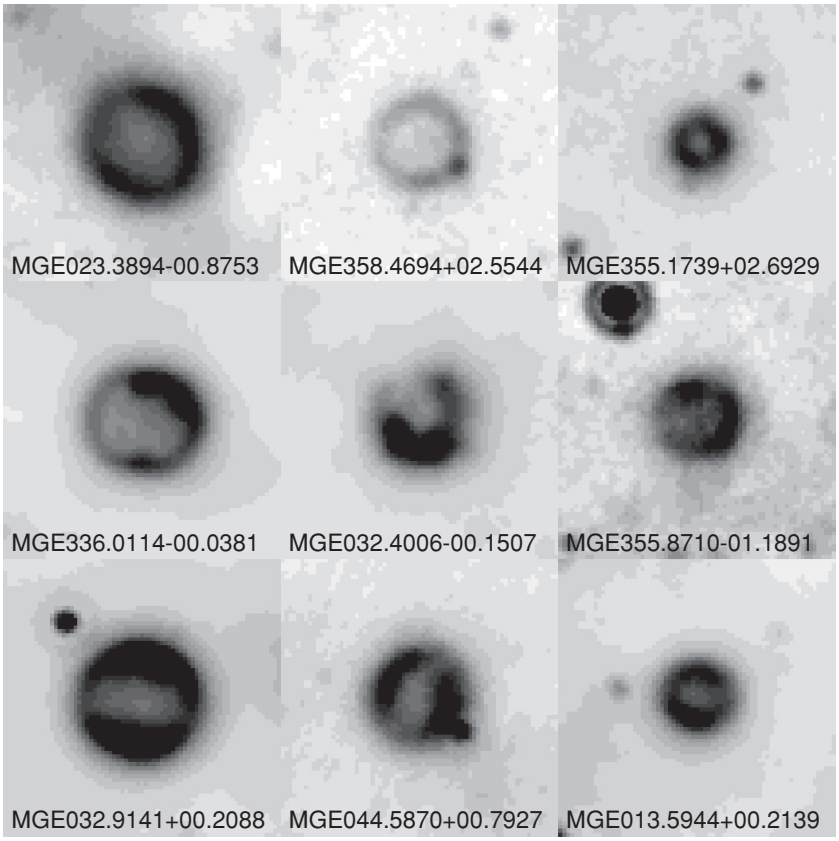

Figure 2. Examples of ring objects. Top row: rings. Middle row: irregular rings. Bottom row: bilaterally symmetric. Each panel is about 1.′5 across.

search for the disks and rings. Figure 6 shows 8 of the 10; the remaining two are possible spiral galaxies and are addressed in the Appendix.

We make no claims regarding completeness of the catalog as a whole or for any of the morphology types, although an effort at a thorough visual search of all the MIPSGAL mosaics was made. Detection depends not only on the complexity and background variation of a given region of the mosaics, which are significant factors in a visual search, but also on the intrinsic properties of the sources themselves. In particular, low surface brightness objects against backgrounds with steep gradients are likely to be missed, although we have not quantified the detection problem.

2.1. Statistical Overview

Of the 416 total objects, we identified 54 objects with central sources, 112 rings, 226 disks, 24 two-lobed objects, plus the two filamentary and 10 miscellaneous objects. Overall, there is slightly more than one object per square degree ($\sim$340 deg^2 in the MIPSGAL survey), with a higher density near the Galactic center ($\sim$2 per square degree for $|l| < 10^\circ$) and lower away (0.85 per square degree for $l > 10^\circ$ and 0.6 per square degree for $l < 350^\circ$). The sensitivity is approximately constant over the entire MIPSGAL survey region.

Figure 7 shows a histogram of the Galactic longitude of the 240 objects with a latitude within 1° of the plane (we have data further from the plane only within 10° of the Galactic center), in 10° bins. There is a clear population enhancement in the Galactic center region, comprising about a quarter of the total, and a general falloff to larger longitudes away from the center. There are also apparent enhancements at about 30° from the center, although the small numbers make it difficult to make definite claims about the distribution. The enhancement at $l \sim 30^\circ$ is about a 2σ deviation from the general trending and is likely a real effect. The enhancement at $l \sim 330^\circ$ is only a 1σ deviation from the mean trending, and is more ambiguous.

Figure 8 shows the two-dimensional (2D) distribution of the objects in Galactic coordinates, separated by the object group. Here all the objects are displayed. The dashed lines show the approximate boundaries of the MIPSGAL survey. The disks show a markedly higher population density at high latitude (>1° from the plane) near the Galactic center, but as we have no high-latitude data elsewhere, interpreting this result is problematic. Also, this increased high-latitude disk density is likely to be at least in part a selection effect as the backgrounds at 24 μm are much more quiescent away from the plane. The rings also show a modest high-latitude enhancement but otherwise seem not to be preferentially located in the plane. The central-source objects by contrast show a definite paucity in the high-latitude data but instead show an evident clustering in regions $\sim$30° from the Galactic center.

Figure 9 shows histograms of the angular sizes of the central-source objects, and the rings and disks combined. The lower limit of about 10″ is dictated by the search criterion that objects be either distinctly ringlike or show a flat profile; objects much below 10″ are either unresolved or barely resolved and thus are generally omitted from consideration due to the typical peaked appearance of such sources. All the rings and disks are below 1′ in diameter, and the vast majority are below 30″, while the median of the central-source objects is 44″. The two-lobed objects are too few to provide a meaningful histogram but generally follow the rings and disks in size range.

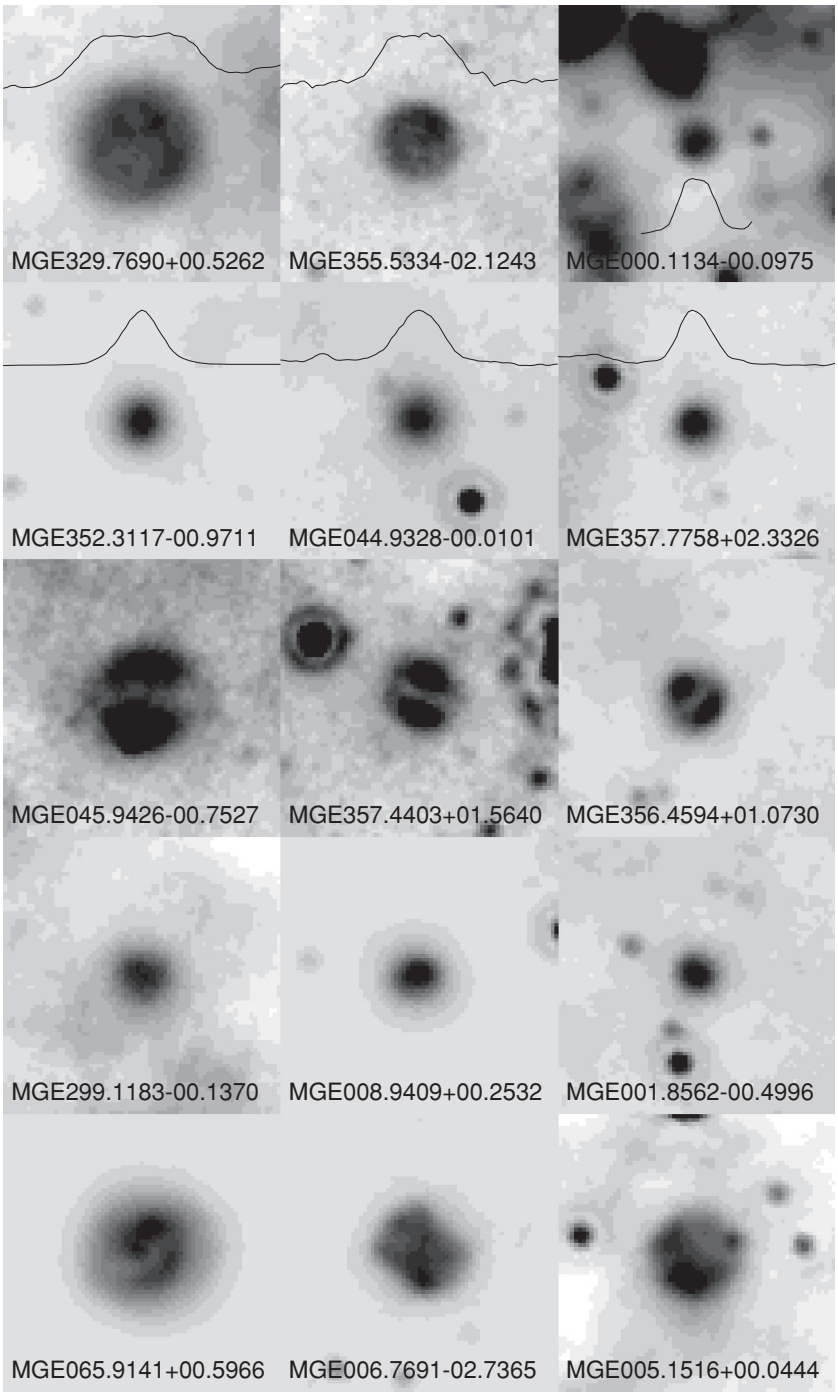

Figure 3. Examples of disk objects. Top to bottom: flat, peaked, bilaterally symmetric, oblong, and irregular. Each panel is about 1.′5 across. The flat and peaked examples also have horizontal slices included to show the distinction between these subgroups.

2.2. Flux Measurements

We performed aperture photometry to determine the 24 μm fluxes of the objects. For this purpose, we used both the original MIPSGAL mosaics and the point-source-subtracted version of the mosaics (S. Shenoy et al. 2010, in preparation). For each object, an ON source radius is selected by examining both the 2D images and 1D vertical and horizontal slices through the center of the object. The ON radius is chosen to minimally contain the entire object.

Similarly, the 2D images and slices are inspected to determine the radii for the OFF annulus, which are selected to match the apparent background surface brightness at the object, avoid nearby sources, and stay as close as possible to the ON radius. The background intensity $I_{\rm BG}$ is determined as the median of the pixels in the OFF annulus. The background is subtracted from the ON circle, the ON pixels are summed, and the sum is scaled by the pixel solid angle (for the MIPSGAL mosaics, $\Omega_{\rm pixel} = 3.67 \times 10^{-11}$ sr) to give the flux F_{24}:

$$F_{24} = \Omega_{\rm pixel} \sum_{i=1}^{n} (p_i - I_{\rm BG}) = \Omega_{\rm pixel} \left(\sum_{i=1}^{n} p_i - n I_{\rm BG} \right), \quad (1)$$

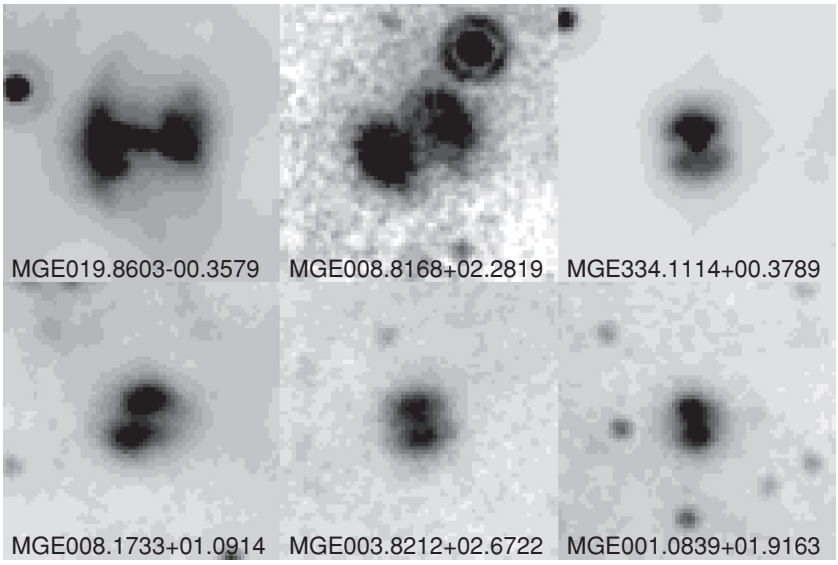

Figure 4. Examples of two-lobed objects. Each panel is about 1.′5 across.

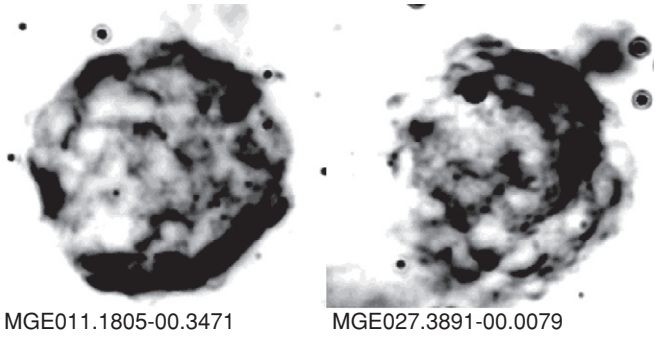

Figure 5. Filamentary objects. Each panel is about 5.′6 across.

where the summation is over the n pixel values p_i in the ON region.

For the central-source objects, the original mosaics are used to determine the fluxes because the source subtraction is not reliable for the central sources (many are not strictly pointlike). The fluxes thus may be occasionally contaminated by other point sources occurring within the ON radius. For the remainder of the objects, and for all background measurements, the source-subtracted mosaics are used.

The flux errors are determined using both the uncertainty map (a product of the mosaic generation in the MOPEX[7] software package) and an empirically measured background error estimate. The uncertainty map provides a per-pixel error estimate ($\sigma_{\mathrm{UNC},i}$) and is presumed to be uncorrelated across pixels. The measurement of the rms over the OFF annulus pixels (σ_{OFF}) reflects both pixel-to-pixel scatter and also variations that are correlated on some length scale due to true background fluctuations. To be conservative, we assume that background fluctuations dominate the OFF annulus rms, and therefore interpret it to be the overall uncertainty in the measured background level I_{BG} assigned to the ON region, and so the error for nI_{BG} is $n\sigma_{\mathrm{OFF}}$.

[7] The MOPEX software is available for download at http://ssc.spitzer.caltech.edu/postbcd/mopex.html.

With these assumptions, the error in the flux is expressed by

$$\sigma_{F_{24}}^2 = \Omega_{\mathrm{pixel}}^2 \left(\sum_{i=1}^{n} \sigma_{\mathrm{UNC},i}^2 + n^2 \sigma_{\mathrm{OFF}}^2 \right). \quad (2)$$

Note that this is an upper limit because we are assuming a worst-case situation for the uncertainty in the background level measurement, which generally dominates the error expression, and also because σ_{OFF} is in part an empirical measure of some noise contributions that are already represented in the uncertainty map for the ON circle (e.g., Poisson noise from the background emission).

3. IRAC AND MIPS 70 μM DETECTIONS

We searched the GLIMPSE images for counterparts in each of the shorter wavelength IRAC bands, as well as the MIPSGAL 70 μm data (R. Paladini et al. 2010, in preparation). GLIMPSE data are available for 314 of the objects. Of these, roughly 14% (44) of the objects are detected at 8 μm with extended emission, 80% (252) were definite non-detections, and the remainder were ambiguous. At 70 μm, data are available for 368 objects, with 19% (60) detections and 46% (149) non-detections (there is a considerable amount of ambiguously associated emission at 70 μm, overlapping with the objects but with no obvious related morphology). Figure 10 shows examples of definite detections, non-detections, and ambiguous detections at 8 μm and 70 μm for three disk objects.

The detection fractions are somewhat higher for the objects with 24 μm central sources. The central sources themselves are observed in all IRAC bands for 94% of these objects. (IRAC central sources are observed for about 11% of the rings, disks, and two-lobed objects.) For extended emission, at 8 μm (50 objects with IRAC data), there are 24% (12) detections and 56% (28) non-detections. At 70 μm (46 objects), there are 43% (20) detections and 15% (7) non-detections.

Figure 11 shows three-color images of four objects using 3.6 μm and 8 μm IRAC data from the GLIMPSE survey (blue and green) and 24 μm MIPSGAL data (red). The upper left panel shows an example where there is no extended emission at 8 μm (although there may be at 70 μm). When present, extended

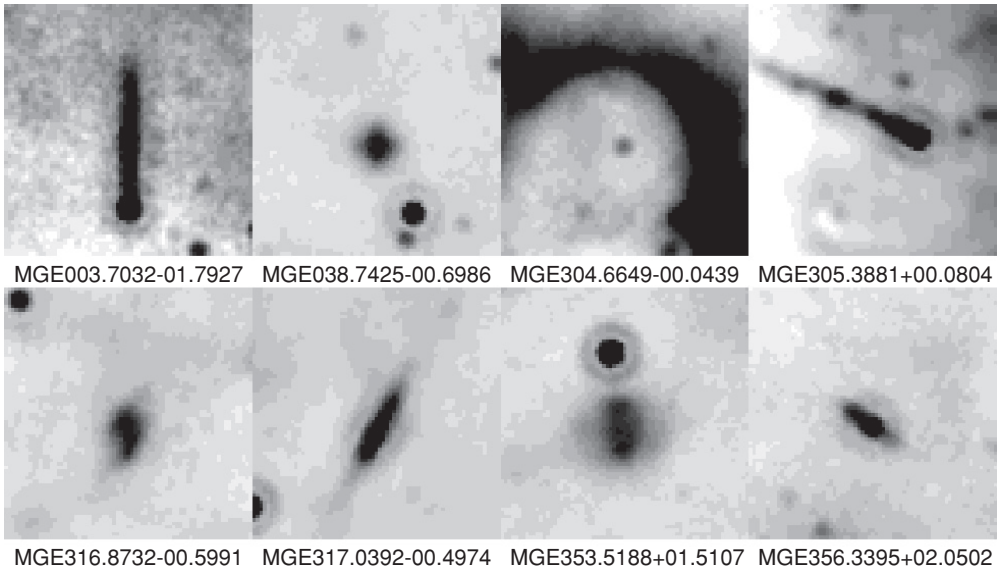

Figure 6. Miscellaneous objects. Each panel is about 1.′5 across. MGE316.8732-00.5991 and MGE317.0392-00.4974 are galaxies identified in the GLIMPSE survey (Jarrett et al. 2007).

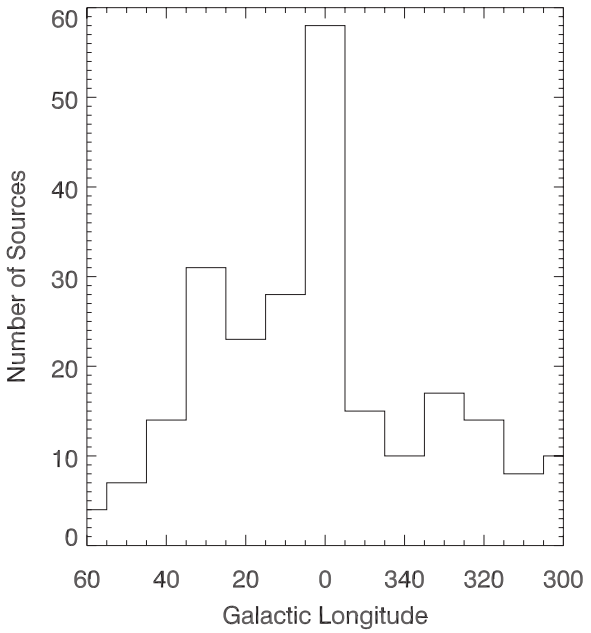

Figure 7. Histogram of Galactic longitudes of objects within 1° of the plane.

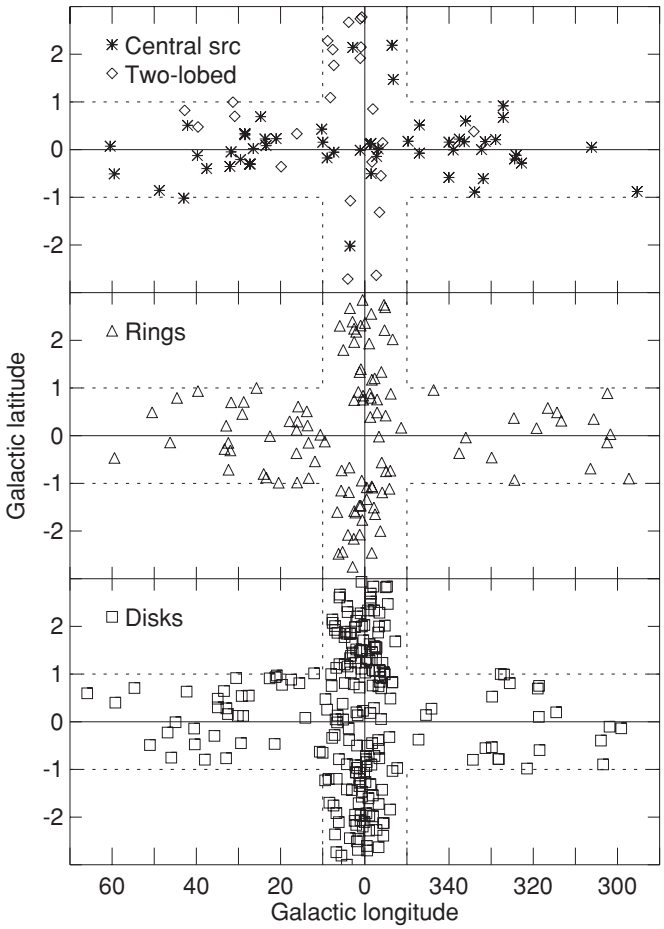

Figure 8. Locations of the catalog objects in Galactic coordinates. The dashed lines show the approximate limits of the MIPSGAL survey.

8.0 μm emission is typically either cospatial (Figure 11, upper right) with the 24 μm emission or interior to it (Figure 11, lower left). In only one instance, shown in the lower right of Figure 11, does the 8.0 μm emission appear to extend beyond the 24 μm structure. In this case, there is fainter emission at 24 μm in the 8 μm region, but the 24 μm structure is dominated by the bright emission that fills the central hole in the 8 μm structure. The average size of the 24 μm structures that also have 8 μm extended emission is $\sim$30″. Thus, in most cases, the relative shapes and sizes of the 8 μm and 24 μm emission regions are readily apparent.

In the cases where the 8 μm and 24 μm emission are cospatial, the emitting particles, presumably large molecules such as polycyclic aromatic hydrocarbons (PAHs) and small grains, respectively, must be well mixed where the structures are well resolved at both wavelengths (the diffraction limits were $\sim$2″ and $\sim$6″ at 8 μm and 24 μm, respectively), as in the examples shown in Figure 11. For the smallest disks and rings, it is harder to say, and these objects could, of course, turn out to be more complex if observed at higher resolution.

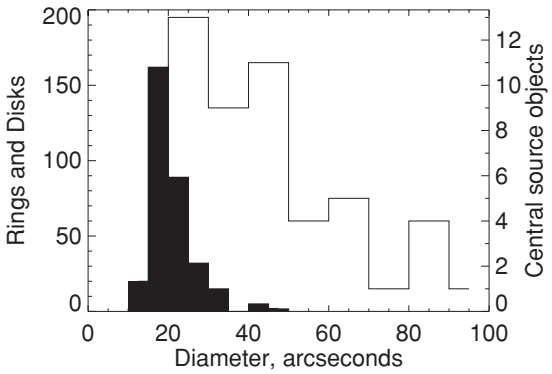

Figure 9. Distribution of object diameters for central-source objects (open histogram) and rings and disks combined (filled histogram).

For those instances where the emission structures are clearly not cospatial, the story is more complicated. Complex emission structures are commonly seen in the visible from PNe, such as the well-known Ring Nebula. That complexity, however, is caused by a variety of ions of different excitation potentials. Here, in a few instances where spectroscopy shows that the 24 μm emission is actually line emission from [O IV], there is no detected 8 μm or 70 μm emission, either pointlike or extended (N. Flagey et al. 2010, in preparation). Chu et al. (2009) observed 36 known Galactic PNe with MIPS, comparing the 24 μm emission with Hα images. They explain the spatial differences between their 24 μm emission and the Hα emission as depending on the dust content and excitation/ionization structures in a particular PN. Here too, the dust density distribution and the spectral energy distribution of the central exciting source are probably also combining to create the observed 8 μm and 24 μm emission structures. The different "layers" of dust emission could represent different episodes of mass loss from the parent star while it was on the AGB. Radiative transfer models (e.g., Egan et al. 1988) that account for the 2D or 3D dust density structures, the spectral energy distribution of the exciting source (which will be quite problematic for the objects where none such has been detected), etc., are needed to fully describe these emission structures, as was done with *Midcourse Space Experiment* (MSX) data for similar objects (e.g., Egan et al. 2002; Clark et al. 2003), but that is beyond the scope of this paper.

4. SIMBAD CORRELATIONS

To help determine the nature of these sources, we did a SIMBAD search around each object.[8] A search radius of 2′

[8] Given the updates that occasionally take place in SIMBAD we note that the searches were performed in 2008 October.

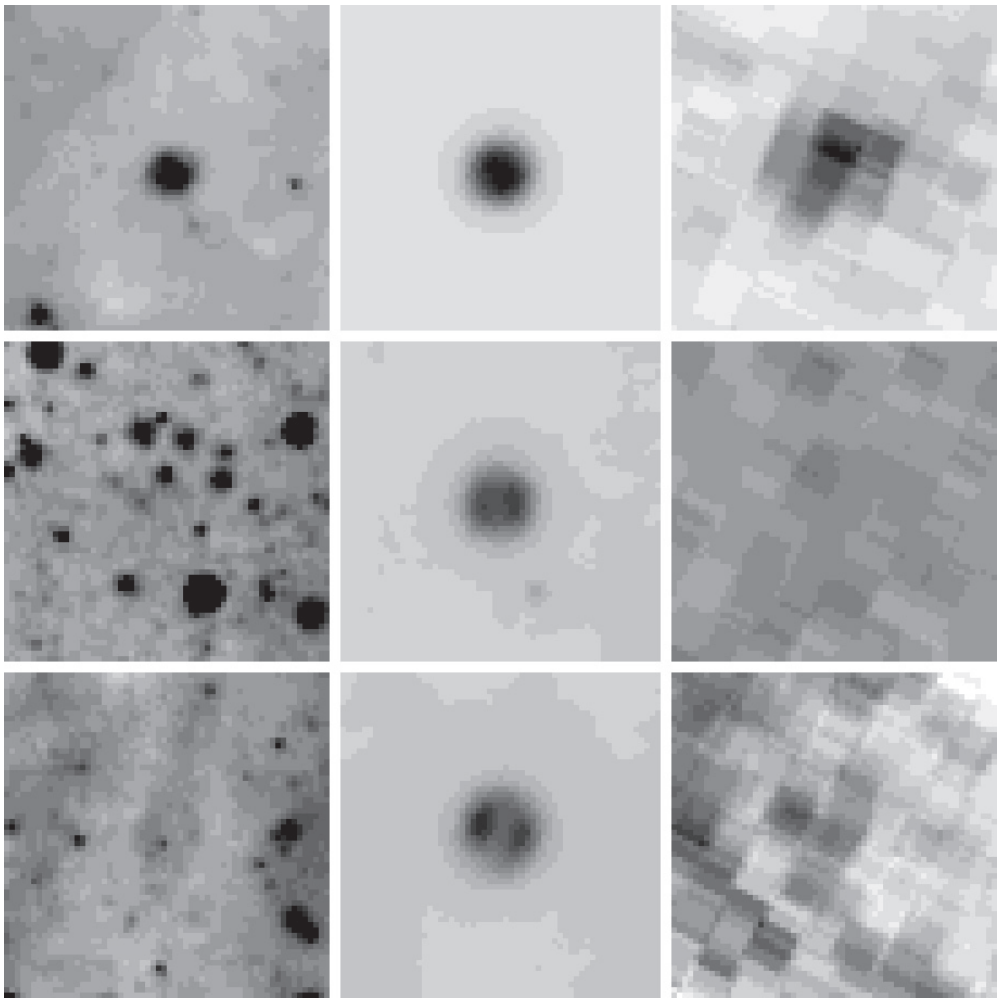

Figure 10. Left to right: 8 μm, 24 μm, and 70 μm images. Top: definite detections at 8 μm and 70 μm for the flat disk MGE030.1503+00.1237. Center: non-detections, bilaterally symmetric disk MGE002.2728-00.9131. Bottom: ambiguous detections, bilaterally symmetric disk MGE007.7506-00.3392. Each panel is approximately 1.′3 across.

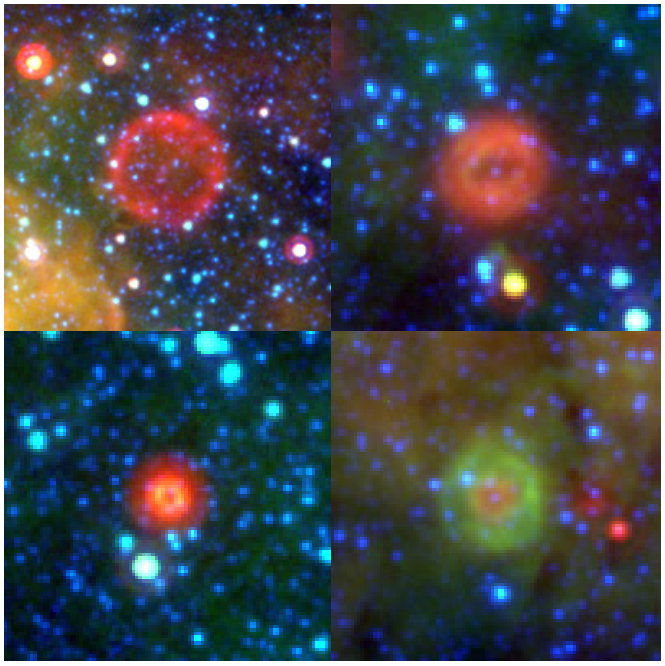

Figure 11. Three-color images of four objects. Red: 24 μm, green: 8 μm, and blue: 3.6 μm. Upper left: MGE015.8261+00.6109, no 8 μm point source or extended emission. Upper right: MGE029.0781+00.4547, 8 μm emission cospatial with the 24 μm emission. Lower left: MGE009.3521+00.4736, a thin ring of 8 μm emission interior to the 24 μm emission. Lower right: MGE337.5950-00.3664, the only instance where the 8 μm emission surrounds the 24 μm structure. The image size for MGE015.8261+00.6109 is $4'.2\times4'.2$; the other three are $2'.1\times2'.1$.

was used to ensure that objects with imprecise coordinates, particularly *IRAS* sources, were not missed. The results were then compared to the 24 μm images to determine if a SIMBAD object correlated with our target or with another object in the field. We found 105 objects out of the 428 (including filamentary and miscellaneous) with a counterpart in SIMBAD. In most cases where a match was judged to be real, the SIMBAD object was within $10''$ from our source coordinates. If an *IRAS* source corresponds to a particular section of one of our sources, such as the brightest arc of a ring, this is noted in the table notes. For the three SNRs, although the pulsar and other components might be closer to the center of the structure we detect, i.e., nominally a closer match to the coordinates, we give the association as the SNR since we are detecting the extended emission, not the pulsar. There are a few objects that were associated with radio sources detected at a single wavelength. These cases are sufficiently unusual that they may reflect chance associations despite being within a few arcseconds of our 24 μm objects.

4.1. Morphology and Source Type

Since approximately three-quarters of our sources are unknown, we can only draw conclusions as to what they are by extension from the sources with known associations. As mentioned above, among the categories returned with the SIMBAD results is the object type. For objects that have been previously studied, a literature search may reveal further information about the object (for example, two luminous blue variables are identified simply as stars by SIMBAD). Here, we describe the kinds of previously identified objects in each of the four main categories.

Objects with central sources. Just under half (24/54) of the objects with central stars have SIMBAD counterparts, associated with either the central source or the extended emission. Eight are associated with emission-line stars, including two luminous blue variables and one post-AGB star. Two others are PNe, one is an SNR, and two are identified as stars, with no further information available in the literature beyond their spectral types (B9 and M2). The remaining 11 are identified only as *IRAS* sources with no additional information available, except perhaps Two Micron All Sky Survey (2MASS)[9] data.

Rings. Of the 112 ring objects, 22 have associations in SIMBAD. Of these, over half (13) are PNe, distributed fairly evenly among the three ring subgroups (given the small numbers involved). Six more are *IRAS* sources, two are radio wavelength objects, and one is a B9 star. As with the central star objects, these nine have no additional references.

Disks. The SIMBAD associations among the 226 disk objects are predominantly PNe: 36 of the 42 objects with counterparts are PNe. The remainder include three otherwise anonymous *IRAS* sources, two radio wavelength objects, and one eclipsing binary.

Two-lobed. Only five of the 30 two-lobed objects have SIMBAD counterparts. Two are PNe identified in the Macquerie/AngloAustralian Observatory/Strasbourg Hα PN survey (Parker et al. 2006; Miszalski et al. 2008). Two have an *IRAS* association with no other information available. The last is associated with a star in the young open cluster NGC 6383, and as with the small number of radio sources, may be a chance spatial coincidence.

5. THE CATALOG

Table 1 is the catalog of all the objects. The table is divided into object group and subgroups, and within each subgroup the objects are sorted by increasing Galactic longitude.

Name. Constructed on the Galactic longitude and latitude.

J2000 Coordinates. The centers of the objects were selected by eye and specified as the nearest pixel in the MIPSGAL mosaics, so the precision for the coordinates is good to about $2''$.

Diameter. The boundaries of the objects are evaluated by eye in the mosaics, and the diameter on the horizontal axis (for round objects) is specified as the nearest integral pixel span, converted to arcseconds and rounded to integral values. For objects with irregular boundaries, the larger of the horizontal and vertical axes is used.

24 μm flux. The flux calculation is described in Section 2.2. The errors calculated from Equation (2) are shown as percentages. Errors greater than or equal to 100% are truncated to 99%.

Detection flags. These are determined by visual inspection of the 8 μm GLIMPSE images and 70 μm MIPSGAL images. For point sources, an affirmative result ("Y") required a point source at the geometric center of the object and be free of confusion. An ambiguous result ("?") is indicated if a source is slightly off-center or there is confusion present. A negative result ("N") means clearly no point source present. A dash means no data are available. For extended emission, an affirmative result required a morphology similar to the 24 μm morphology (or at least concentric), an ambiguous result means some local extended emission present but of uncertain correspondence to the 24 μm emission, and a negative result means either no

[9] Most of the catalog sources have at least one 2MASS source within $5''$, often more than one, which is not surprising given the density of sources in the Galactic plane. However, unless there is a corresponding point source at IRAC wavelengths, a chance alignment cannot be ruled out.

Table 1
MIPSGAL Disk and Ring Catalog

Name	J2000 Coordinates		Diam.	F_{24}	Detection Flags			SIMBAD Associations		
	$\alpha(^{h\,m\,s})$	$\delta(^{\circ\,\prime\,\prime\prime})$	($''$)	(Jy)	8 μm Point	8 μm Ext.	70 μm Ext.	Dist. ($''$)	Name	Object Type
(1)	(2)	(3)	(4)	(5)	(6)	(7)	(8)	(9)	(10)	(11)
1a: objects with central sources—regular										
MGE002.8493+02.1430	17 44 05.3	−25 23 16	24	0.04(15)	...	...	?			
MGE003.5216-02.0237	18 01 36.1	−26 55 40	21	0.04(24)	...	...	N			
MGE007.3429-00.0549	18 02 22.3	−22 38 00	32	1.1(80)	Y	Y	...			
MGE008.9460-00.1750	18 06 13.1	−21 17 45	15	0.13(35)	Y	N	?	1.5	HD 313771	*
MGE009.9541+00.1556	18 07 05.2	−20 15 16	28	0.35(18)	Y	?	?			
MGE010.2114+00.4289	18 06 36.2	−19 53 48	40	18.(< 1)	Y	Y[k]	Y	4.3	IRAS 18036-1954	PN?
MGE021.0510+00.2292	18 28 41.5	−10 27 06	45	0.29(99)	Y	N	N			
MGE023.4499+00.0820	18 33 43.4	−08 23 35	25	1.7(34)	Y	N	?			
MGE023.6857+00.2226	18 33 39.5	−08 07 08	44	3.7(29)	Y	N	?			
MGE024.7290+00.6910	18 33 55.3	−06 58 38	50	11.(4)	Y	Y	Y	1.1	V* V481 Sct	LBV

Note. [k] Extended emission seen in all IRAC bands.
(This table is available in its entirety in machine-readable and Virtual Observatory (VO) forms in the online journal. A portion is shown here for guidance regarding its form and content.)

localized extended emission present or emission that is clearly not associated with the object.

SIMBAD associations. These columns show the SIMBAD associations as described above. In about a dozen cases, two probable associations are present, typically a PN coincident with our coordinates, plus an *IRAS* source that is almost certainly the same object but has not been noted as such in SIMBAD. In these cases, the primary identification is given as the PN or star, and the *IRAS* association is indicated in a footnote. Five objects were matched with separate searches in the catalogs in the VizieR service which are not yet incorporated into SIMBAD; these are noted in footnotes.

6. DISCUSSION

While spectroscopic study would be necessary to determine the physical nature of any given object, we may draw some tentative conclusions based on the known identifications. It is striking that for the rings, disks, and two-lobed objects, nearly all of the specific SIMBAD identifications (50 of 57) are either PNe or PN candidates, and the remainder are identified as either stars or radio sources, which do not preclude these objects from being PNe as well. The objects in the catalog have been selected solely on the basis of their 24 μm morphology, and without prior knowledge or expectation of what any of these objects are, so it is tempting to conclude from the near-universality of the PN identifications that the ring, disk, and two-lobed lists collectively form a catalog of PNe in the MIPSGAL survey region, specifically PNe that are both observed and resolved at the 6″ 24 μm MIPS resolution.

This catalog could therefore contain up to 300 previously undiscovered PNe, helping us to alleviate the known discrepancy between the number of expected Galactic PNe and the number that have been identified (e.g., Parker et al. 2003; Phillips & Ramos-Larios 2008), which can, at least in part, be attributed to extinction effects that are largely absent at 24 μm. It is also possible, however, that the unidentified objects are located preferentially deeper in the Galactic disk, and some portion of them may be massive evolved stars or other object types observed from a great distance rather than garden-variety PNe.

The completeness of this tentative PN catalog (rings, disks, and two-lobed objects) is limited by the general exclusion of centrally peaked objects, whether the selection of "irregular" objects encompasses the actual range of morphological PN variation, and the vagaries of a visual search of a large image set. PNe can be strongly peaked at 24 μm; see Su et al. (2004) for an example that most likely would have been excluded from our catalog for that reason. Of the 35 "peaked" disks in the list, all 7 with identifications are PNe, so this suggests that there are many more such objects that have been omitted from the catalog. Circularly symmetric, centrally peaked extended objects are perhaps 10–15 times more numerous in the MIPSGAL data than the rings and disks selected for this catalog, but this larger ensemble certainly includes objects such as YSOs (see, e.g., Cyganowski et al. 2008, for some examples) and unresolved sources at 24 μm.

In contrast to the ubiquitous identification of the ring and disk objects as PNe, Morris et al. (2006) present an outer Galaxy object discovered in the *Spitzer* Galactic First Look Survey morphologically similar at 24 μm to the objects selected for this catalog (we would categorize it as an irregular ring). Spectroscopy showed that this object lacks a dust continuum; virtually all the 24 μm emission is attributed to [O IV]. These authors interpret this object as a young SNR. This object is slightly larger in angular extent, about 1′, than the largest of our rings and disks, but not enough to argue that it is in a separate class of objects. In other gross properties (low surface brightness, lack of detection in IRAC bands and 70 μm), it is similar to many of our ring and disk objects. Spectroscopic data for one of our irregular ring objects, MGE059.4354-00.4662, also show a lack of a dust continuum (Billot et al. 2009), and whose 24 μm signature is also due to ionized oxygen.

Chu et al. (2009) compared MIPS 24 μm observations of Galactic PNe with archival Hα and He II data. They suggest that the 24 μm emission is a combination of dust continuum emission and the [O IV] line at 25.9 μm, where the relative contributions depend on the ionization and dust density structure of the PN in question. Additional *Spitzer* Infrared Spectrometer (IRS; Houck et al. 2004) observations of a small sample of ring and disk sources will help determine the emission mechanisms in the present catalog (N. Billot et al. 2010, in preparation; N. Flagey et al. 2010, in preparation).

The objects with central sources form an ensemble distinct from the sourceless rings and disks. While two are identified

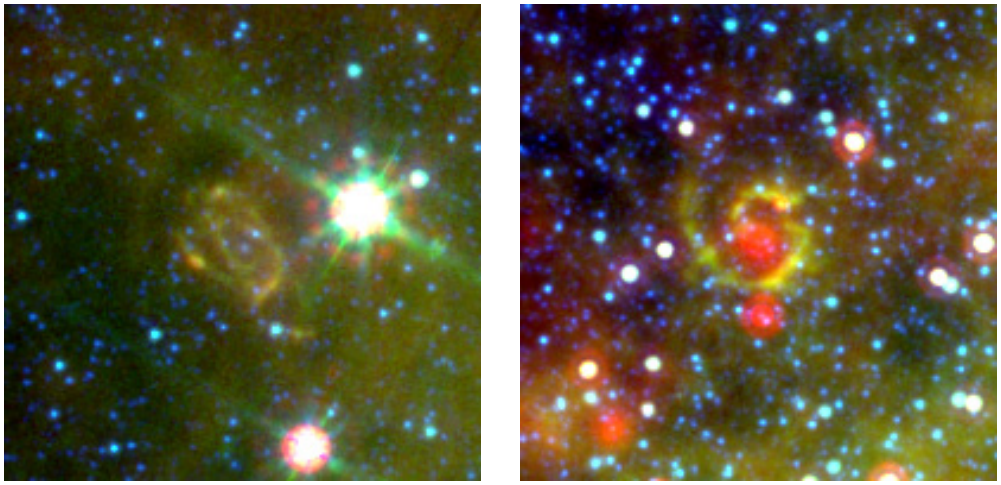

Figure 12. Left: three-color image of MGE314.2378+00.9793. Red: 24 μm, green: 8 μm, and blue: 3.6 μm. There is 8 μm and 24 μm emission from the central source but it is dominated by the 3.6 μm emission with this stretch. The bright star to the right is IRAS 14195-5938. Right: three-color image of MGE351.2381-00.0145.

as candidate PNe, the majority of the identifications (apart from the generic IR sources) are that of the central stars, and a preponderance of these are emission-line stars.

While the visibility of the residual star in a PN at 24 μm is generally not anticipated, Su et al. (2007) report a bright central pointlike source at 24 μm in the Helix Nebula, which they attribute to an unresolved debris disk surrounding the white dwarf. The two identified central-source PN candidates in our catalog fall in the angular size range of the rings and disks, and so this could be a plausible interpretation for the smaller of the unidentified central-source objects, but the majority of the central-source objects have a significantly larger angular size than even the largest rings and disks (or identified PNe among them), and so this interpretation should not be assumed for the central-source objects in general without further evidence (a debris disk model is more likely for the peaked disks in our catalog.).

We therefore attempt no general interpretation of the central-source objects except to speculate that they are all evolved objects. One interesting characteristic is their Galactic distribution: the apparent clustering at 30° from the Galactic center corresponds to the tangent points of the molecular ring. If these objects are largely confined to the molecular ring then this suggests that they are evolved stages of massive, short-lived stars.

This work is based on observations made with the *Spitzer Space Telescope*, which is operated by the Jet Propulsion Laboratory, California Institute of Technology under a contract with NASA. Support for this work was provided by NASA in part through an award issued by JPL/Caltech. This research made use of the SIMBAD database and the VizieR catalog access tool, operated by the Centre de Données Astronomique de Strasbourg. This research has also made use of NASA's Astrophysics Data System Bibliographic Services.

Facilities: Spitzer (MIPS)

APPENDIX

TWO POSSIBLE NEW SPIRAL GALAXIES

As mentioned in the main text, in addition to the sources with a strong degree of circular or bipolar symmetry, we also noted a number of other unusually shaped objects. Of particular note are the two objects shown in Figure 12. Each shows remarkable spiral structure at both 24 μm and 8 μm; neither has a counterpart found in SIMBAD.

For MGE314.2378+00.9793, the extended ($\sim$45″ × 80″ at 24 μm) spiral emission is prominent at 24 μm and 8 μm, and faintly visible at 5.8 μm. The central region appears dominated by 3.6 μm emission, although there is a central point source present in all five bands. In contrast, the central region of MGE351.2381-00.0145 is dominated by a blob of 24 μm emission ($\sim$13″) that is completely absent at the shorter wavelengths. The spiral structure, $\sim$75″ across at 24 μm, is detected at 5.8 μm as well as 8 μm and 24 μm. There also appears to be 70 μm emission associated with MGE351.2381-00.0145.

One possibility is that these are two spiral galaxies previously hidden due to their location behind the Galactic plane. This seems particularly plausible for MGE351.2381-00.0145, located at $(l, b) = (351.24, -0.01)$; MGE314.2378+00.9793 is at a slightly higher latitude, $(l, b) = 314.24, +0.99)$, but still well within the plane. Both are in rich star fields, as evidenced by the numerous 3.6 μm sources in the figure. MGE314.2378+00.9793 coincides with an 843 MHz radio continuum source from the Sydney University Molongo Sky Survey (Bock et al. 1999), and MGE351.2381-00.0145 has a radio continuum source at 1.4 GHz from the NRAO VLA Sky Survey (NVSS; Condon et al. 1998). The location of MGE314.2378+00.9793 is also coincident with the Norma Wall of galaxies, about a degree from the two galaxies recently found with IRAC by the GLIMPSE team (Jarrett et al. 2007). (Those two galaxies, MGE316.8732-00.5991 and 317.0392-00.4974, are actually two of the three objects in the "miscellaneous" group with SIMBAD associations.) Follow-up observations to determine their radial velocities would be necessary to test this scenario for the two spiral sources.

A second possibility for MGE314.2378+00.9793 is that there are two rings superimposed, with one rotated about 30°. One trouble with this, though, is that while there is a point source reasonably well centered in the overall structure, there do not seem to be point sources near the center of either of the potential separate ring structures.

An alternative explanation for MGE351.2381-00.0145 is some kind of rotating wind mechanism, creating a pinwheel nebula comparable to that around Wolf–Rayet stars such as WR 104 (Tuthill et al. 1999) or WR 98a (Monnier et al. 1999). The lack of a point source at the center does not really support

that, though, as well as the fact that the angular size of the MGE351.2381-00.0145 nebula, several hundred times the $\sim 0\farcs2$ of WR 104, makes the WR interpretation unlikely. On the other hand, we know of no spiral galaxies with such strong central emission at 24 μm yet not at 8 μm.

Another "miscellaneous" object, MGE356.3395+02.0502, shown in Figure 6, is a central point source with a bright bar of emission plus a fainter halo above and below the bar. It, too, is an NVSS point source, and could be a smaller or more distant spiral seen edge-on, rather than face-on as with the first two objects. Unfortunately, at $(l, b) \sim 356.34, 2.05$, it was outside the GLIMPSE coverage. Again, additional observations are needed to determine what this source actually is.

MGE305.3881+00.0804 has a morphological similarity to photoablating proplyd candidates observed at optical wavelengths in Orion (O'Dell et al. 1993) and the Carina Nebula (Smith et al. 2003). The Wolf–Rayet star WR 48a is about $2'$ distant and is approximately aligned with the head–tail orientation of this object. At a distance of 4 kpc, the $\sim 1'$ tail is $\sim$1 pc in length, $\sim$100 times that of the Orion proplyds and $\sim$10 times those in Carina, which suggests that this could be a much more massive protoplanetary disk than those found in Orion or Carina.

MGE003.7032-01.7927 resembles a proplyd, but there is no apparent source driving the flow. A jet could be a possibility, but this is nothing like a YSO protostellar jet, and there is no signature of a counter jet.

REFERENCES

Benjamin, R. A., et al. 2003, PASP, 115, 953
Billot, N., Flagey, N., Noriega-Crespo, A., Shenoy, S., Mizuno, D., Kraemer, K., & Latter, B. 2009, BAAS, 41, 762
Bock, D. C.-J., Large, M. I., & Sadler, E. M. 1999, AJ, 117, 1578
Carey, S. J., et al. 2009, PASP, 121, 76
Chu, Y.-H., et al. 2009, AJ, 138, 691
Churchwell, E., et al. 2006, ApJ, 649, 759
Clark, J. S., Egan, M. P., Crowther, P. A., Mizuno, D. R., Larianov, V. M., & Arkharov, A. 2003, A&A, 412, 185
Condon, J. J., Cotton, W. D., Greisen, E. W., Yin, Q. F., Perley, R. A., Taylor, G. B., & Broderick, J. J. 1998, AJ, 115, 1693
Cyganowski, C. J., et al. 2008, AJ, 136, 2391
Egan, M. P., Clark, J. S., Mizuno, D. R., Carey, S. J., Steele, I. A., & Price, S. D. 2002, ApJ, 572, 288
Egan, M. P., Leung, C. M., & Spagna, G. F., Jr. 1988, Comput. Phys. Commun., 48, 271
Fazio, G., et al. 2004, ApJS, 154, 10
Gehrz, R. D. 1989, in IAU Symp. 135, Interstellar Dust, ed. L. J. Allamandola & A. G. G. M. Tielens (Dordrecht: Kluwer), 445
Helfand, D. J., Becker, R. H., White, R. L., Fallon, A., & Tuttle, S. 2006, AJ, 131, 2525
Houck, J., et al. 2004, ApJS, 154, 18
Jarrett, T. H., et al. 2007, AJ, 133, 979
Miszalski, B., Parker, Q. A., Acker, A., Birkby, J. L., Frew, D. J., & Kovacevic, A. 2008, MNRAS, 384, 525
Mizuno, D. R., et al. 2008, PASP, 120, 1028
Monnier, J. D., Tuthill, P. G., & Danchi, W. C. 1999, ApJ, 525, L97
Morris, P. W., et al. 2006, ApJ, 640, L179
O'Dell, C. R., Wen, Z., & Hu, X. 1993, ApJ, 410, 696
Olnon, F. M., et al. 1986, A&AS, 65, 607
Parker, Q., et al. 2003, in IAU Symp. 209, Planetary Nebulae: Their Evolution and Role in the Universe, ed. S. Kwok, M. A. Dopita, & R. Sutherland (San Francisco, CA: ASP), 25
Parker, Q. A., et al. 2006, MNRAS, 373, 79
Phillips, J. P., & Ramos-Larios, G. 2008, MNRAS, 386, 995
Rieke, G., et al. 2004, ApJS, 154, 25
Smith, N., Bally, J., & Morse, J. 2003, ApJ, 587, L105
Su, K. Y. L., et al. 2004, ApJS, 154, 302
Su, K. Y. L., et al. 2007, AJ, 657, L41
Tuthill, P. G., Monnier, J. D., & Danchi, W. C. 1999, Nature, 398, 487
Walker, R., & Price, S. D. 1975, AFCRL-TR-75-0373
White, R. L., Becker, R. H., & Helfand, D. J. 2005, AJ, 130, 586